analytical chemistry

Article

pubs.acs.org/ac

Morphology-Driven Control of Metabolite Selectivity Using Nanostructure-Initiator Mass Spectrometry

Jian Gao,[†,‡,∥] Katherine B. Louie,[†,‡] Philipp Steinke,[§] Benjamin P. Bowen,[†,‡] Markus de Raad,[†,‡] Ronald N. Zuckermann,[∥] Gary Siuzdak,[⊥] and Trent R. Northen*[,†,‡]

[†]Environmental Genomics and Systems Biology Division and [∥]The Molecular Foundry, Lawrence Berkeley National Laboratory, 1 Cyclotron Road, Berkeley, California 94720, United States

[‡]Joint Genome Institute, Department of Energy, 2800 Mitchell Drive, Walnut Creek, California 94598, United States

[§]Fraunhofer Institute for Photonic Microsystems IPMS - Center Nanoelectronic Technologies (CNT), Königsbrücker Strasse 178, 01099 Dresden, Germany

[⊥]Scripps Center for Metabolomics & Departments of Chemistry, Molecular and Computational Biology, The Scripps Research Institute, 10550 North Torrey Pines Road, La Jolla, California 92037, United States

Supporting Information

ABSTRACT: Nanostructure-initiator mass spectrometry (NIMS) is a laser desorption/ionization analysis technique based on the vaporization of a nanostructure-trapped liquid "initiator" phase. Here we report an intriguing relationship between NIMS surface morphology and analyte selectivity. Scanning electron microscopy and spectroscopic ellipsometry were used to characterize the surface morphologies of a series of NIMS substrates generated by anodic electrochemical etching. Mass spectrometry imaging was applied to compare NIMS sensitivity of these various surfaces toward the analysis of diverse analytes. The porosity of NIMS surfaces was found to increase linearly with etching time where the pore size ranged from 4 to 12 nm with corresponding porosities estimated to be 7−70%. Surface morphology was found to significantly and selectively alter NIMS sensitivity. The small molecule (<2k Da) sensitivity was found to increase with increased porosity, whereas low porosity had the highest sensitivity for the largest molecules examined. Estimation of molecular sizes showed that this transition occurs when the pore size is <3× the maximum of molecular dimensions. While the origins of selectivity are unclear, increased signal from small molecules with increased surface area is consistent with a surface area restructuring-driven desorption/ionization process where signal intensity increases with porosity. In contrast, large molecules show highest signal for the low-porosity and small-pore-size surfaces. We attribute this to strong interactions between the initiator-coated pore structures and large molecules that hinder desorption/ionization by trapping large molecules. This finding may enable us to design NIMS surfaces with increased specificity to molecules of interest.

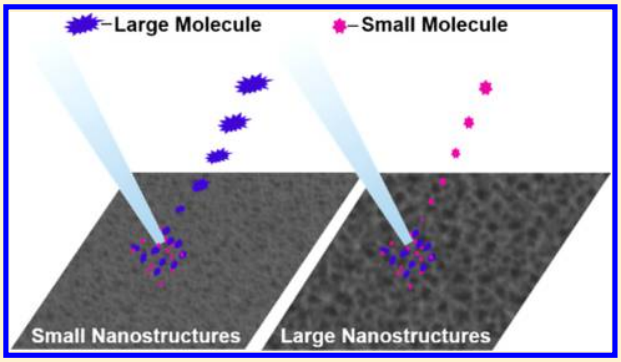

Mass spectrometry (MS) is an important analytical platform for metabolomic studies because it offers quantitative analyses with high sensitivity and the possibility of diagnosing metabolites' chemical structures.[1−3] MS in combination with chromatography has been widely applied in metabolite analysis due to its high mass accuracy and reproducibility. However, the complicated sample preparation as well as potential adducts limits its application in screening large metabolite libraries. Matrix-assisted laser desorption/ionization (MALDI) is a high throughput MS technique that provides a fast and sensitive analysis of metabolites with masses above 700 Da.[4−6] Matrix interference can become problematic when detecting molecules in the low mass range.[4]

To overcome the limitations of MALDI, the surface-assisted laser desorption ionization (SALDI) technique that utilizes nanostructured surfaces instead of a conventional matrix to assist analyte laser desorption ionization (LDI) has been developed to expand the detectable mass range of metabolites.[3,4,7] A large diversity of nanomaterials, such as porous surfaces,[8,9] carbon nanotubes,[10,11] nanowires,[12] nanopost arrays (NAPA),[3,13,14] and thin films,[15,16] have been reported as functional interfaces to promote the analyte desorption/ionization process. As one of the most tested SALDI techniques, NIMS has demonstrated the capability to analyze a broad range of molecules and biological tissues.[17−20] This surface-based mass analysis technique relies on its liquid "initiator"-coated nanostructure surface to efficiently absorb

Received: February 16, 2017
Accepted: May 18, 2017
Published: May 18, 2017

DOI: 10.1021/acs.analchem.7b00599
Anal. Chem. 2017, 89, 6521−6526

and transfer laser energy to analyte ions during initiator vaporization.[9]

Surface morphology of NIMS substrates play an essential role in the desorption/ionization process of analyte molecules and thus determines the substrates' sensitivity of transferring intact molecules into gas-phase ions.[21−25] As reported previously, NIMS signal is highly dependent on laser intensity, which suggests that efficient energy conversion happens during surface restructuring of NIMS substrates driving desorption/ionization.[3,26,27] However, the relationship between surface morphologies and NIMS performance toward different analytes is largely unexplored. Improved understanding on how NIMS surface morphology influences its sensitivity toward specific analytes has the potential to guide the developments of NIMS surfaces designed for increased metabolite coverage or potentially selective metabolite analysis.[2,4,28]

Hydrofluoric acid (HF) electrochemical etching as well as inductively coupled plasma (ICP) reactive ion etching (RIE) has been introduced to generate nanostructured silicon surfaces for NIMS.[21,27] ICP-RIE etching shows an advantage for fabricating high sensitivity NIMS surfaces in a safe and high-throughput operation. There are many determining factors regarding this fabrication process, such as plasma generator power, etching chamber temperature, and total gas flow rates and ratios that can dramatically influence the surface morphology of etched substrates.[27,29−32] Although it is desirable to avoid HF given the associated hazards, the electrochemical etching approach enables production of desired surface morphologies by sampling the etching duration.[21,33−36] The larger number of variables impacting surface structures using ICP-RIE etching conditions makes it difficult to gradually tune the surface structures.

Here we investigate the relationship of surface morphologies and NIMS sensitivity toward diverse analytes. Electrochemical etching at a constant current for different durations was used to create nanostructure surfaces with 4−12 nm pores. The NIMS sensitivity of this series of NIMS substrates was analyzed using a variety of analytes, revealing pore-size-dependent analyte selectivity. These findings have the potential to enable the designs of NIMS substrates designated for target molecules.

EXPERIMENTAL SECTION

Materials. Arginine (m/z 175.12 ± 0.01 Da), palmitoylcarnitine (m/z 400.34 ± 0.01 Da), streptomycin (m/z 582.27 ± 0.01 Da), and insulin chain B oxidized (insulin B, m/z 3496.62 ± 0.01 Da) were purchased from Sigma-Aldrich (St. Louis, MO). Bradykinin (m/z 904.47 ± 0.01 Da), angiotensin (m/z 1296.68 ± 0.01 Da), neurotensin (m/z 1672.92 ± 0.01 Da), ACTH (clip 1−17) (m/z 2093.09 ± 0.01 Da), ACTH (clip 18−39) (m/z 2465.20 ± 0.01 Da), and ACTH (clip 7−38) (m/z 3657.92 ± 0.01 Da) were purchased from AnaSpec (Fremont, CA) as a premixed peptide mass standard kit. The compounds were each dissolved in a 1:1 methanol (J. T. Baker, LC-MS grade) to water (J. T. Baker, LC-MS grade) solution with 0.1% formic acid added (Sigma-Aldrich, MS grade) to reach a concentration of 10 mg/L. All the chemicals were of high purity grade and were not further purified. It is important to note that mass concentrations, common in mass spectrometry, were used in this study, thus favoring detection of the small molecules. While this does not change the overall trends, we provide Supporting Information Table 1 to enable comparison of molar concentrations.

NIMS Substrate Fabrication. Surfaces were processed as described in detail elsewhere.[21] Briefly, prime grade silicon wafers (4″ diameter, 525 μm thickness, p-type with resistivity of 0.01−0.02 ohm/cm, backside oxide seal removed) were purchased from Addison Engineering (Fremont, CA). The wafers were trimmed into 7.0 cm squares and then cleaned in three solvent baths: trichloroethylene, acetone, and methanol for 15 min sequentially. The cleaned wafers were placed in a custom Teflon etching chamber with HF etching bath (24% HF, 26% water, 50% ethanol) and electrochemically etched at 2.36 A with etching times of 2, 3.5, 5, 10, 15, 20, 25, 30, 35, and 40 min, in duplicates. The etched wafers were soaked with the initiator BisF17 (Gelest, Morrisville, PA) for 1 h and used as NIMS substrates after removing the extra initiator with a nitrogen gun, again as described in ref 7.[21]

Surface Analysis. A Zeiss Ultra 60-SEM (Oberkochen, Germany) was used to visualize the surface morphologies of these NIMS substrates, and the spectroscopic ellipsometer (Semilab SOPRA EP5, North Billerica, MA)[37−39] was used to measure the optical properties of etched porous surfaces. Pore size and porosity of these surfaces were calculated using Winelli II software with the Forouhi−Bloomer model.[40−42] An acoustic printer (EDC ATS-100) was used to deposit 10 nL of each analyte solution onto NIMS surfaces. The dimension of printed sample spots is ∼400 μm diameter.[43] An AB Sciex (Foster City, CA) TOF/TOF 5800 MALDI mass spectrometer configured at positive ionization mode was used for NIMS imaging of sample spot arrays with the step size of 50 μm, and the acquired data were converted and plotted using OpenMSI.[44]

RESULTS AND DISCUSSION

The correlation of different surface morphologies and their performance in NIMS analysis of diverse analytes were explored in this study. A series of silicon substrates with different surface morphologies were fabricated via electrochemical etching, and their NIMS sensitivity toward diverse analytes was examined using mass spectrometry imaging.

Electrochemical Etching To Control Surface Morphology. The anodic electrochemical etching method was used here to create nanostructured features on the monocrystalline silicon surface in a HF bath.[45] The rate of pore formation was kept constant by fixing HF concentration, electric current density, and silicon wafer properties. The duration of the etching process was varied from 2 to 40 min to adjust the surface morphologies of this series of etched substrates.

SEM images of these silicon substrates with etching times of 2, 10, 25, and 40 min are shown in Figure 1A−D (see Supporting Information for the bulk of SEM images). These images show that porous structures are distributed homogeneously over the entire etched surface, and that the pore size gradually increases with etching time. These porous nanostructures enable large surface area as well as low melting points that allow efficient conversion of analyte molecules into gas-phase ions under low intensity laser irradiation.[3,26,27,46]

Spectroscopic ellipsometry was applied to characterize physical parameters of these porous substrates, and adsorption and desorption isotherms of toluene in the silicon surface were obtained under a broad range of relative pressures (sample pressure/saturated pressure) as shown in Supporting Information. The results were fitted by the Kelvin equation and Forouhi−Bloomer's model to extract their pore size distribution from these isotherms (Supporting Information).[40−42] The calculated porosity, pore size, and thickness of the porous films

DOI: 10.1021/acs.analchem.7b00599
Anal. Chem. 2017, 89, 6521−6526

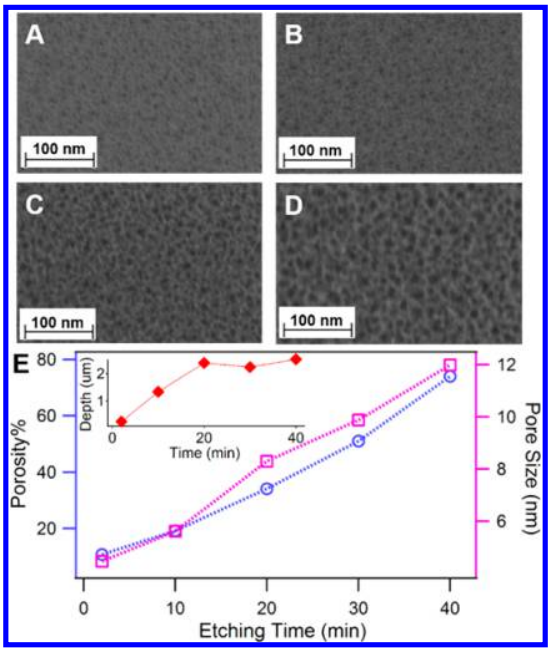

Figure 1. SEM images of etched silicon surfaces obtained at variable etching durations: (A) 2 mins; (B) 10 min; (C) 25 mins; (D) 40 min. (E) The correlations between surface morphologies of NIMS substrates and etching time: porosity in blue, pore size in purple. The inset shows the trend of etched depth with etching time.

are presented in Figure 1E. Both pore size and porosity of these substrates linearly increase with etching time, consistent with the observations by SEM. The pore size of these substrates shows a gradual increase from ~4 to 12 nm while their porosity increases from ~7% to 70% of the total etched volume. The etching depth of these porous substrates sharply rises from ~250 nm to 2.4 μm and then fluctuates in the range of 2.2 μm to 2.5 μm.

Morphology-Dependent NIMS Selectivity Behavior. This series of nanostructured silicon substrates were coated with BisF17 initiator and further examined as NIMS surfaces using chemically and physically diverse analytes. The analytes ranged from 174 to 3657 Da and included arginine, palmitylcarnitine, streptomycin, bradykinin, angiotensin, neurotensin, ACTH residues ("clip" 1–17, 18–39, 7–38), and insulin B. Ten nanoliters of each analyte solution was deposited onto the various NIMS surfaces using acoustic printing. This enabled multiple replicates to control spot-to-spot variations over the same NIMS surface. Mass spectrometry imaging was performed for data acquisition, and raw data analysis was performed using OpenMSI software.[44]

An example of the resulting data is shown in Figure 2. It includes 10 sets of 20 replicate sample spots of the analyte ACTH (clip 18–39) printed on 10 different NIMS surfaces with increasing pore size. The average intensity of mass spectra corresponding to ACTH (clip 18–39) is plotted with error bars on the right side of Figure 2. From this analysis, it is apparent that ACTH (clip 18–39) shows a strong dependency on the NIMS surface morphologies. Its signal intensity gradually increases with the etching time of substrates and reaches a maximum at 15 min, and afterward it gradually decreases. This observation indicates that the desorption/ionization process of this molecule highly relies on the surface structures of silicon substrates.

NIMS sensitivity of this series of nanostructured silicon substrates was examined with the complete panel of analyte molecules via imaging mass, as illustrated in Figure 2 for ACTH (clip 18–39), using 20 sample spots of each analyte acoustically printed onto these substrates. Mass spectra of these sample spots were averaged, and their NIMS peak intensities are shown in Figure 3. To determine statistically significant changes in intensity, a single factor ANOVA was performed on the averaged NIMS signals for each analyte from these NIMS substrates, followed by a posthoc two-sample t test (Table 1, Supporting Information). This analysis showed, not surprisingly, that etching time is a significant factor in determining the signal intensity for all analytes examined.

Importantly, the ACTH peptides are subsets of the same peptide and therefore represent some control of analyte chemistry. Despite their different molecular weights and molecular sizes, they show strikingly similar signal dependence on porosity as well as an optimal signal at 15 min etching corresponding to an average pore size of 7 nm and porosity of 29% (Figure 3). In contrast, insulin B shows the strongest signal on substrates etched for only 2 min (pore size, 4 nm; porosity, 7%), and no NIMS signal can be detected with

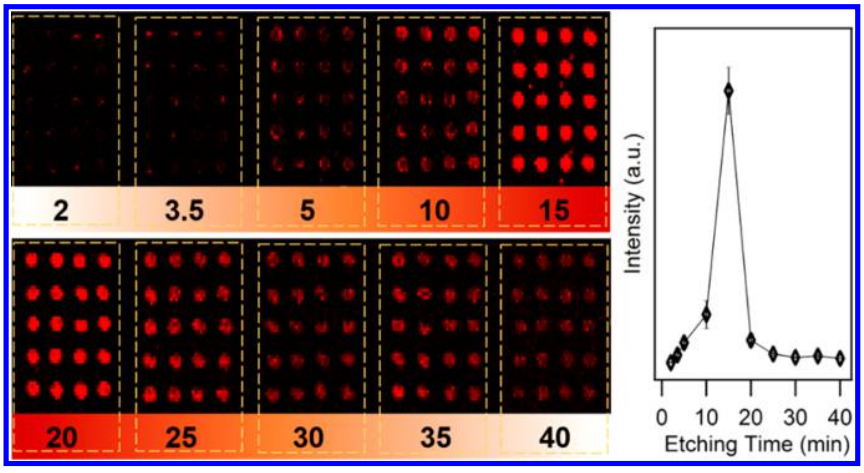

Figure 2. NIMS sensitivity comparison of the analyte ACTH (clip 18–39) using silicon substrates obtained at different etching times from 2 to 40 min.

DOI: 10.1021/acs.analchem.7b00599
Anal. Chem. 2017, 89, 6521–6526

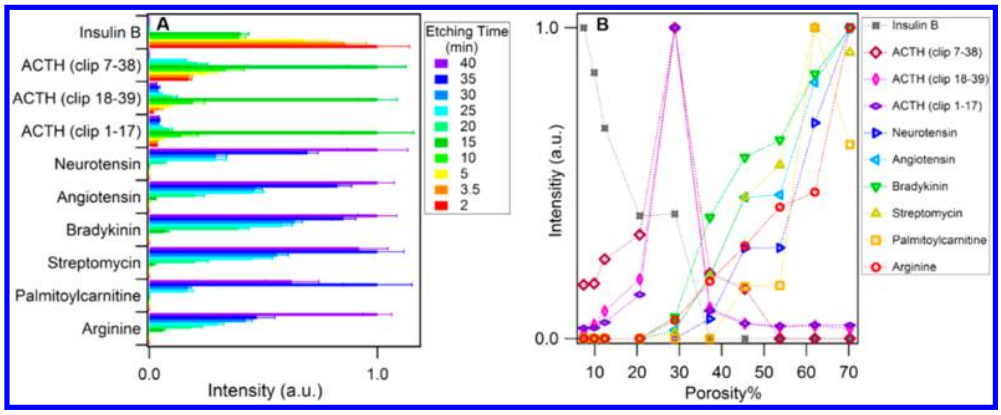

Figure 3. NIMS sensitivity study of nanostructured silicon substrates etched at 2 to 40 min using a variety of molecules (n = 20). (A) Histogram of NIMS signals showing their intensity change by the substrates' etching time (the corresponding scatter plot is included in Supporting Information), (B) Scatter plot of NIMS signals by the substrates' porosity.

etching times longer than 20 min. Moving from 2 to 15 min etching time increases ACTH peptide signal 5.8 fold and decreases insulin B signal 2.5 fold. In contrast, analytes with molecular weight smaller than 2000 Da, despite their chemical diversity (arginine, palmitoylcarnitine, streptomycin, bradykinin, and angiotensin), showed similar signal response to etching time and are only detectable with the substrates etched at 15 min or longer with the highest signal at 35 and 40 min.

These results provide evidence of the strong coupling between NIMS surface morphology and desorption/ionization efficiency of analytes. NIMS substrates fabricated at short etching time (≤15 min) have the highest sensitivity for the largest molecules (e.g., insulin B) while the substrates fabricated at long etching time (≥15 min) reveal high performance on ionizing small molecules. Reassuringly, the etching time most widely used for NIMS, 15 min, represents an intermediate value and in our view represents the best overall surface morphology for the range of molecules we evaluated.

We can speculate as to the mechanisms that drive this selectivity. Previous studies investigating the mechanisms of desorption−ionization from porous silicon (DIOS) suggested that surface melting may trigger the efficient release of surface-adsorbed analyte and that surfaces with higher porosity had lower laser-induced melting temperatures and higher sensitivity for the very small decylamine families.[26] Here we examine NIMS surfaces where the surface nanostructures are coated/filled with initiator. It is found that substrates fabricated at long etching time that have the highest porosity and therefore large surface area did indeed have the highest sensitivity for small molecules (Figure 3). This is consistent with the view of a surface energy-driven process, where increased surface area results in more efficient desorption/ionization. The surprising behavior of the largest peptides may reflect a strong interaction between initiator-coated nanostructures and the analytes that interferes with the desorption/ionization process. In this case, the combination of small pores has decreased adsorption energies and can provide more explosive and directed release of energy required by large analyte molecules during their desorption/ionization.

To further examine the possibility that the size of analytes relative to the pore size may explain the dramatic decrease in sensitivity for the high molecular weight peptides, we estimated the molecular spatial conformations. Optimized Chem3D structures showed the spatial lengths of analytes range from 1 to 4 nm (Supporting Information); thus, they are on the same scale of the pore sizes of this series of NIMS surfaces (Figure 4). Unfortunately, we do not know the thickness of the initiator

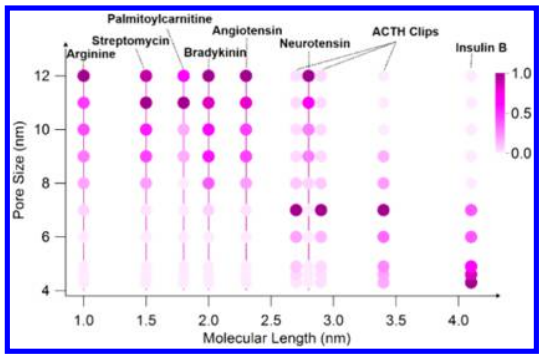

Figure 4. Correlation of pore sizes and molecular length regarding NIMS sensitivity. Note: Signal is normalized to the maximum intensity for each analyte.

coating; however, coated porous features on silicon surfaces could turn into physical traps during the surface melting process and cage analyte molecules inside NIMS surfaces. This trapping effect would become more severe when the spatial dimensions of molecules become comparable to the initiator-coated pore sizes. The substrates obtained at short etching time have small pores (<7 nm) and low porosity (<25%), allowing large molecules to sit on top of the nanostructures and thus avoiding "trapping". We anticipate that this trapping behavior would be highly dependent on the surface chemistry, offering the exciting possibility that this affinity could be tuned to selectively desorb/ionize analytes of interest, as suggested by the surprising behavior of the ACTH peptides.

CONCLUSION

We observe a pore-size-dependent analyte selectivity for NIMS. High sensitivity for small molecules is observed for larger pores while small pores show higher sensitivity for large molecules. These observations are thought to reflect physical interactions of analyte molecules and NIMS surfaces. NIMS surface restructuring is the essential energy source to the desorption/ionization of small molecules while large molecules highly rely on the direct physical contact with NIMS top surfaces to absorb directed release of laser energy without becoming trapped

DOI: 10.1021/acs.analchem.7b00599
Anal. Chem. 2017, 89, 6521−6526

within the pores. Consistent with this view, analyte chemical properties is likely another major factor that determines adsorptive forces. To further understand this morphology-dependent selectivity behavior, a very important future research direction is to examine the sensitivities of different nanostructured surfaces with a broad range of metabolites as well as their mixtures in a complex matrix. Although the exact mechanism is unclear, these findings suggest the exciting possibility of "tuning" NIMS surfaces to trap interferences among other applications.

■ ASSOCIATED CONTENT

Supporting Information

The Supporting Information is available free of charge on the ACS Publications website at DOI: 10.1021/acs.analchem.7b00599.

Table of molarities, SEM images, adsorption/desorption isotherms, pore size distributions, scatter plots, table of statistical analysis and optimized geometries of metabolites (PDF)

■ AUTHOR INFORMATION

Corresponding Author

*E-mail: TRNorthen@lbl.gov.

ORCID

Markus de Raad: 0000-0001-8263-9198

Ronald N. Zuckermann: 0000-0002-3055-8860

Trent R. Northen: 0000-0001-8404-3259

Notes

The authors declare no competing financial interest.

■ ACKNOWLEDGMENTS

This work is supported by Defense Advanced Research Projects Agency (DARPA) Fold F(x) program, and the U.S. Department of Energy Office of Science award DE-SC0014079 to UC Berkeley, the Samuel Noble Foundation, University of Oklahoma. Work at the Molecular Foundry was supported under U.S. Department of Energy contract no. DE-AC02-05CH11231.

■ REFERENCES

(1) Scalbert, A.; Brennan, L.; Fiehn, O.; Hankemeier, T.; Kristal, B. S.; van Ommen, B.; Pujos-Guillot, E.; Verheij, E.; Wishart, D.; Wopereis, S. *Metabolomics* **2009**, *5*, 435−458.

(2) Korte, A. R.; Stopka, S. A.; Morris, N.; Razunguzwa, T.; Vertes, A. *Anal. Chem.* **2016**, *88*, 8989−8996.

(3) Stolee, J. A.; Walker, B. N.; Zorba, V.; Russo, R. E.; Vertes, A. *Phys. Chem. Chem. Phys.* **2012**, *14*, 8453−8471.

(4) Guinan, T.; Kirkbride, P.; Pigou, P. E.; Ronci, M.; Kobus, H.; Voelcker, N. H. *Mass Spectrom. Rev.* **2015**, *34*, 627−640.

(5) Karas, M.; Krüger, R. *Chem. Rev.* **2003**, *103*, 427−440.

(6) Dreisewerd, K. *Chem. Rev.* **2003**, *103*, 395−426.

(7) Chen, C.-T.; Chen, Y.-C. *Anal. Chem.* **2005**, *77*, 5912−5919.

(8) Wei, J.; Buriak, J. M.; Siuzdak, G. *Nature* **1999**, *399*, 243−246.

(9) Northen, T. R.; Yanes, O.; Northen, M. T.; Marrinucci, D.; Uritboonthai, W.; Apon, J.; Golledge, S. L.; Nordstrom, A.; Siuzdak, G. *Nature* **2007**, *449*, 1033−1036.

(10) Pan, C.; Xu, S.; Zou, H.; Guo, Z.; Zhang, Y.; Guo, B. *J. Am. Soc. Mass Spectrom.* **2005**, *16*, 263−270.

(11) Xu, S.; Li, Y.; Zou, H.; Qiu, J.; Guo, Z.; Guo, B. *Anal. Chem.* **2003**, *75*, 6191−6195.

(12) Coffinier, Y.; Szunerits, S.; Drobecq, H.; Melnyk, O.; Boukherroub, R. *Nanoscale* **2012**, *4*, 231−238.

(13) Stopka, S. A.; Rong, C.; Korte, A. R.; Yadavilli, S.; Nazarian, J.; Razunguzwa, T. T.; Morris, N. J.; Vertes, A. *Angew. Chem., Int. Ed.* **2016**, *55*, 4482−4486.

(14) Walker, B. N.; Stolee, J. A.; Pickel, D. L.; Retterer, S. T.; Vertes, A. *J. Phys. Chem. C* **2010**, *114*, 4835−4840.

(15) Nayak, R.; Knapp, D. R. *Anal. Chem.* **2010**, *82*, 7772−7778.

(16) Grechnikov, A. A.; Georgieva, V. B.; Alimpiev, S. S.; Borodkov, A. S.; Nikiforov, S. M.; Simanovsky, Y. O.; Dimova-Malinovska, D.; Angelov, O. I. *J. Phys. Conf. Ser.* **2010**, *223*, 012038.

(17) Kurczy, M.; Northen, T.; Trauger, S.; Siuzdak, G. In *Mass Spectrometry Imaging of Small Molecules*; He, L., Ed.; Springer: New York, 2015; pp 141−149.

(18) Calavia, R.; Annanouch, F. E.; Correig, X.; Yanes, O. *J. Proteomics* **2012**, *75*, 5061−5068.

(19) Louie, K. B.; Bowen, B. P.; Cheng, X.; Berleman, J. E.; Chakraborty, R.; Deutschbauer, A.; Arkin, A.; Northen, T. R. *Anal. Chem.* **2013**, *85*, 10856−10862.

(20) Moening, T. N.; Brown, V. L.; He, L. In *Mass Spectrometry Imaging of Small Molecules*; He, L., Ed.; Springer: New York, 2015; pp 151−157.

(21) Woo, H.-K.; Northen, T. R.; Yanes, O.; Siuzdak, G. *Nat. Protoc.* **2008**, *3*, 1341−1349.

(22) Louie, K.; Northen, T. In *Mass Spectrometry in Metabolomics*, Raftery, D., Ed.; Springer: New York, 2014; pp 313−329.

(23) Xiao, Y.; Retterer, S. T.; Thomas, D. K.; Tao, J.-Y.; He, L. *J. Phys. Chem. C* **2009**, *113*, 3076−3083.

(24) Yoon, S. H.; Gamage, C. M.; Gillig, K. J.; Wysocki, V. H. *J. Am. Soc. Mass Spectrom.* **2009**, *20*, 957−964.

(25) Abdelmaksoud, H. H.; Guinan, T. M.; Voelcker, N. H. *ACS Appl. Mater. Interfaces* **2017**, *9*, 5092−5099.

(26) Northen, T. R.; Woo, H.-K.; Northen, M. T.; Nordström, A.; Uritboonthail, W.; Turner, K. L.; Siuzdak, G. *J. Am. Soc. Mass Spectrom.* **2007**, *18*, 1945−1949.

(27) Gao, J.; de Raad, M.; Bowen, B. P.; Zuckermann, R. N.; Northen, T. R. *Anal. Chem.* **2016**, *88*, 1625−1630.

(28) Lowe, R. D.; Szili, E. J.; Kirkbride, P.; Thissen, H.; Siuzdak, G.; Voelcker, N. H. *Anal. Chem.* **2010**, *82*, 4201−4208.

(29) Jansen, H. V.; de Boer, M. J.; Unnikrishnan, S.; Louwerse, M. C.; Elwenspoek, M. C. *J. Micromech. Microeng.* **2009**, *19*, 033001.

(30) Jiang, F.; Keating, A.; Martyniuk, M.; Prasad, K.; Faraone, L.; Dell, J. M. *J. Micromech. Microeng.* **2012**, *22*, 095005.

(31) Steglich, M.; Käsebier, T.; Zilk, M.; Pertsch, T.; Kley, E.-B.; Tünnermann, A. *J. Appl. Phys.* **2014**, *116*, 173503.

(32) Nguyen, K. N.; Basset, P.; Marty, F.; Leprince-Wang, Y.; Bourouina, T. *J. Appl. Phys.* **2013**, *113*, 194903.

(33) Unagami, T. *J. Electrochem. Soc.* **1980**, *127*, 476−483.

(34) Zhang, X. G.; Collins, S. D.; Smith, R. L. *J. Electrochem. Soc.* **1989**, *136*, 1561−1565.

(35) Kim, H.; Cho, N. *Nanoscale Res. Lett.* **2012**, *7*, 408−408.

(36) Dubey, R. S.; Gautam, D. K. *Superlattices Microstruct.* **2011**, *50*, 269−276.

(37) Bolotov, V. V.; Davletkil'deev, N. A.; Korotenko, A. A.; Roslikov, V. E.; Sten'kin, Y. A. *Tech. Phys.* **2011**, *56*, 1593−1598.

(38) Gaillet, M.; Guendouz, M.; Ben Salah, M.; Le Jeune, B.; Le Brun, G. *Thin Solid Films* **2004**, *455*−*456*, 410−416.

(39) Pickering, C.; Beale, M. I. J.; Robbins, D. J.; Pearson, P. J.; Greef, R. *J. Phys. C: Solid State Phys.* **1984**, *17*, 6535.

(40) Liu, Y.; Xu, G.; Song, C.; Weng, W.; Du, P.; Han, G. *Thin Solid Films* **2007**, *515*, 3910−3913.

(41) Keita, A. S.; Naciri, A. E.; Delachat, F.; Carrada, M.; Ferblantier, G.; Slaoui, A. *Phys. Status Solidi C* **2010**, *7*, 418−422.

(42) Wongmanerod, C.; Zangooie, S.; Arwin, H. *Appl. Surf. Sci.* **2001**, *172*, 117−125.

(43) Greving, M.; Cheng, X.; Reindl, W.; Bowen, B.; Deng, K.; Louie, K.; Nyman, M.; Cohen, J.; Singh, A.; Simmons, B.; Adams, P.; Siuzdak, G.; Northen, T. *Anal. Bioanal. Chem.* **2012**, *403*, 707−711.

(44) Rübel, O.; Greiner, A.; Cholia, S.; Louie, K.; Bethel, E. W.; Northen, T. R.; Bowen, B. P. *Anal. Chem.* **2013**, *85*, 10354−10361.

DOI: 10.1021/acs.analchem.7b00599
Anal. Chem. 2017, 89, 6521−6526

(45) Korotcenkov, G. *Porous Silicon: From Formation to Application: Formation and Properties, Vol. One: Formation and Properties*; CRC Press: Boca Raton, FL, 2016.
(46) Korotcenkov, G. *Porous Silicon: From Formation to Application: Biomedical and Sensor Applications, Vol. Two: Biomedical and Sensor Applications*; CRC Press: Boca Raton, FL, 2016.

DOI: 10.1021/acs.analchem.7b00599
Anal. Chem. 2017, 89, 6521−6526